

Identifying Individual Disease Dynamics in a Stochastic Multi-pathogen Model From Aggregated Reports and Laboratory Data

Yury E. García, Oksana A. Chkrebtii, Marcos A. Capistrán,
Daniel E. Noyola *

July 19, 2022

Abstract

Influenza and respiratory syncytial virus are the leading etiologic agents of seasonal acute respiratory infections around the world. Medical doctors usually base the diagnosis of acute respiratory infections on patients' symptoms, and do not always conduct laboratory tests necessary to identify individual viruses due to cost constraints.

This limits the ability to study the interaction between specific etiological agents

* **Yury E. Garcís** is PhD Student in Applied Mathematics at Centro de Investigación en Matemáticas A.C., Jalisco S/N Col. Valenciana, CP: 36240, Guanajuato, Gto. México (E-mail: yury@cimat.mx). **Oksana A. Chkrebtii** is Assistant Professor at Department of Statistics, The Ohio State University, 1958 Neil Ave, Columbus, OH 43210 (E-mail: oksana@osu.edu). **Marcos Capistrán** is Professor of Mathematics at Centro de Investigación en Matemáticas A.C., Jalisco S/N Col. Valenciana, CP: 36240, Guanajuato, Gto. México (E-mail: marcos@cimat.mx). **Daniel E. Noyola** is Research Professor at Department of Microbiology, Faculty of Medicine, Universidad Autónoma de San Luis Potosí, Av. venustiano Carranza 2405, CP 78210, San Luis Potosí, México (E-mail: dnoyola@uaslp.mx). This research was supported in part by the Mathematical Biosciences Institute (MBI) and the National Science Foundation under grant DMS 1440386. The authors thank Grzegorz A. Rempala (MBI) and Leticia Ramirez (CIMAT) for helpful comments and suggestions. The authors also thank The Ohio State University and Centro de Investigación en Matemáticas (CIMAT).

responsible for illnesses and make public health recommendations. We establish a framework that enables the identification of individual pathogen dynamics given aggregate reports and a small number of laboratory tests for influenza and respiratory syncytial virus in a sample of patients, which can be obtained at relatively small additional cost. We consider a stochastic Susceptible-Infected-Recovered model of two interacting epidemics and infer the parameters defining their relationship in a Bayesian hierarchical setting as well as the posterior trajectories of infections for each illness over multiple years from the available data. We conduct inference based on data collected from a sentinel program at a general hospital in San Luis Potosí, Mexico, interpret the results, and make recommendations for future data collection strategies. Additional simulations are conducted to further study identifiability for these models. Supplementary materials are provided online.

Keywords: Acute respiratory disease, Bayesian hierarchical modeling, Linear noise approximation, Influenza, Respiratory syncytial virus

1 INTRODUCTION

Acute respiratory infections (ARI) are infections of the upper and lower respiratory tract caused by multiple etiological agents. The most frequent causes of these infections are viruses such as adenovirus, influenza A and B, parainfluenza, respiratory syncytial virus (RSV), and rhinovirus. An important public health concern around the world, ARI are responsible for substantial mortality and morbidity (Thompson et al. 2003; Ávila Adarne and Castellanos 2013), mainly affecting children under 5 and adults above 65 years of age (Kuri-Morales et al. 2006). Although different viruses are responsible for ARI, a substantial part of the burden of ARI in most regions is due to influenza and RSV (Chan et al. 2014; Velasco-Hernández et al. 2015; Chaw et al. 2016). The interaction and temporal dynamics of these pathogens are complex. Evidence suggests that influenza and RSV are seasonally related (Mangtani et al. 2006; Bloom-Feshbach et al. 2013) and circulate at similar times of the year in some temperate zones (Bloom-Feshbach et al. 2013; Velasco-Hernández et al. 2015). While it has been shown that these viruses are antigenically unrelated, there is a known dependence between their outbreaks. Because of their interaction and interference, these infections do not usually reach their epidemic peaks simultaneously (Ånestad 1987; Anestad et al. 1982; Anestad and Nordbo 2009), with peak times typically differing by less than one month (Bloom-Feshbach et al. 2013). Additionally, epidemic behavior of influenza has changed with the introduction of vaccination programs (Anestad et al. 1982; Velasco-Hernández et al. 2015), but a vaccine for RSV is not yet available (Modjarrad et al. 2016). In the clinical setting, it is difficult to determine which pathogen may be responsible

for a patient's ARI, because of their overlapping circulation times and similar symptoms. Furthermore, laboratory tests necessary for identification of the virus are not conducted in most patients (Chan et al. 2014). Knowledge of the underlying mechanisms of spread and transmission of these two pathogens and the impact of control measures aids policy makers in assessing public health strategies and decision-making (Huppert and Katriel 2013).

Mathematical modeling has become a powerful tool to study epidemic behaviors in order to predict, assess and control disease outbreaks (Star and Moghadas 2010; Huppert and Katriel 2013; Siettos and Russo 2013). Such models are predominantly stochastic, reflecting the random nature of a large number of human interactions which enable infections to spread and individuals to change their infection status. The probabilities of discrete transitions from one infection state to another are defined up to a set of unknown parameters, which are inferred from observed data. The most widely used models are variations on the "Susceptible-(Exposed-)Infected-Recovered" (SIR/SEIR) formulation, which describes the temporal evolution of the proportion of individuals in each infection state at a given time. A number of strategies have been developed to incorporate process-specific demographic stochasticity in this compartmental model. For example, Dukic et al. (2012) model process stochasticity by an additive white noise process on the growth rate of the infectious population computed from states that evolve according to the deterministic compartmental dynamics described above. In a different approach, Farah et al. (2014) assume additive process noise on the infection states of a deterministic SEIR model. Another approach is taken by Shrestha et al. (2011) by modeling infection state counts as multinomial processes

with probabilities of inclusion obtained by first solving the ODE corresponding to the compartmental model and then solving for the transition probabilities as functions of current states. In this paper, we consider a first-principles stochastic kinetic interpretation of SIR dynamics (Wilkinson 2006; Komorowski et al. 2009; Golightly and Wilkinson 2011; Golightly et al. 2015). This approach accurately reflects inherent stochasticity in a multi-pathogen model because it naturally describes individual-level transitions as stochastic processes incorporating assumptions about these interactions. Since data typically consists of observed infected counts rather than individual transition times, computation of the likelihood requires considering this model in the large volume limit via diffusion approximation (Van Kampen 1992).

Any unknown parameters and forcing functions defining the transition probabilities must be estimated from partially observed and often aggregated infection report data. Because the data and the model are defined on different scales, identification of parameters is not always possible. Additionally, when multiple diseases with similar symptoms are in circulation, particular disease trajectories may not even be distinguishable. In general, the ability to identify parameters and distinguish pathogens depends on both the model structure and the availability and form of the data used to estimate them (Huppert and Katriel 2013). Shrestha et al. (2011) showed via simulation that likelihood-based methods can identify parameters of a multi-pathogen system under some conditions for models where the states are defined by a Multinomial process with expectation given by the solution of an ODE initial value problem. In this work, we consider a first-principles

stochastic kinetic model of the multi-epidemic dynamics and take a Bayesian perspective to quantify uncertainty in estimation and resolve sample paths corresponding to individual epidemics. This approach is particularly important in weakly identified models, but also allows placing both hard and soft constraints on parameters, which often ameliorates identifiability problems in data-poor scenarios.

We aim to separately identify the dynamics of influenza and RSV using aggregate report data and laboratory samples in a stochastic multi-pathogen model developed to describe their time-evolution and interaction. A background process consisting of other ARI-causing pathogens is modeled independently of influenza and RSV. We introduce a strategy to estimate parameters in such multi-pathogen models from aggregate data and show that it is possible to distinguish the dynamics of each virus involved in the infection when even a small sample of additional laboratory data is available.

The article is organized as follows. The motivating application and the data will be described in Section 2. Section 3 begins by constructing a stochastic kinetic model for the evolution of individual infection states of influenza and RSV and then describes the large population limit approximation for this model. A Bayesian hierarchical model is formulated relating the dynamic model to two datasets. Section 4 describes the results of the analysis as well as two simulation studies which shed light on model identification under different data availability scenarios. Finally, Section 5 discusses the feasibility of our approach, summarizes our findings, and offers some perspectives on future work. Software

to reproduce all results is provided at github.com/ochkrebtii/Identifying-ARI-dynamics (upon publication).

2 MOTIVATING APPLICATION

Though our approach is widely applicable, the motivating problem of interest is to identify the dynamics and study the interaction of two ARI-causing viruses in the state of San Luis Potosí, México. It is known that the main viruses in circulation in this area during the annual ARI outbreak are influenza and Respiratory Syncytial Virus (RSV), although other ARI viruses are also reported. In the reported cases, ARI viruses cannot be distinguished based on the physical symptoms alone, and genetic testing to identify the specific pathogen is only done for small samples of certain populations, such as infants.

We use data on weekly ARI recorded during the winter seasons in the years 2002 to 2008 in the state of San Luis Potosí, México. Although data is available from 2000-2010, we excluded from our analysis the year 2009-10, when the global influenza A (H1N1) pandemic caused substantial deviations from the typical patterns of the ARI outbreak. We also excluded years 2000-02 due to lack of laboratory samples for those years. According to the 2010 census, this state had a population of 2,585,518 individuals (Velasco-Hernández et al. 2015). The data analyzed consists of community-based and hospital-based ARI consultation provided by health-care institutions reported to the State Health Service Epidemiology Department (Velasco-Hernández et al. 2015). Each consultation for a new

ARI by a single individual is counted as a report. Additional data comes from a sentinel program that performed virological testing for a small random sample of children under 5 years of age who presented with ARI to identify the specific pathogen causing their illness. This virological surveillance program was established at Hospital Central “Dr. Ignacio Morones Prieto” located in the state capital of San Luis Potosí.

The number of samples processed for viral testing each year was approximately 340. It is important to note that the number of influenza positive samples during the peak week in certain years was very small (fewer than five positive tests). In such cases, we do not expect to be able to identify the effect of each individual pathogen.

3 MODELING

This section begins by describing a first-principles stochastic kinetic model of influenza and RSV dynamics, as well as its diffusion approximation in the large volume limit, required to compute the likelihood of reported infection data. We then construct a Bayesian hierarchical model that relates the governing equations to the two types of data described above.

3.1 Stochastic Dynamical Model of a two-Pathogen System

Stochasticity is inherent in biological systems due to their discrete nature and the occurrence of random natural, environmental, and demographic events. In the case of disease dynamics,

the occurrence of events such as interactions between individuals that constitute exposure can be reasonably described as stochastic. Therefore it is reasonable to model this stochasticity directly in the individual transitions, in contrast to indirectly modeling their aggregate behavior or perturbing a deterministic compartmental model. Stochastic Kinetic or Chemical Master Equation modeling (Allen 2008; Wilkinson 2011) is a mathematical formulation of Markovian stochastic processes, given by a system of differential equations which describe the evolution of the probability distribution of finding the system in a given state at a specified time (Gillespie 2007; Thomas et al. 2012).

To model the relationship between influenza and RSV (henceforward called pathogens 1 and 2 respectively) during a single year, we consider a closed population of size Ω , assumed to be well mixed and homogeneously distributed, where the individuals interacting in a fixed region can make any of \mathcal{R} possible transitions. The stochastic “Susceptible-Infected-Recovered” (SIR) model with two pathogens (Kamo and Sasaki 2002; Adams and Boots 2007; Vasco et al. 2007) is described by eight compartments corresponding to distinct immunological statuses. Denote by $X_{kl}(t)$ the *number of individuals* at time t in immunological status $k \in \{S, I, R\}$ for pathogen 1 and immunological status $l \in \{S, I, R\}$ for pathogen 2. Although simultaneous infection by both viruses is biologically possible, the probability of this event is so small that we choose to omit the state X_{II} from the model.

Our goal in this work is the identification of specific illnesses in a realistically data poor scenario. For this reason, we try to avoid needless complexity in modeling transitions

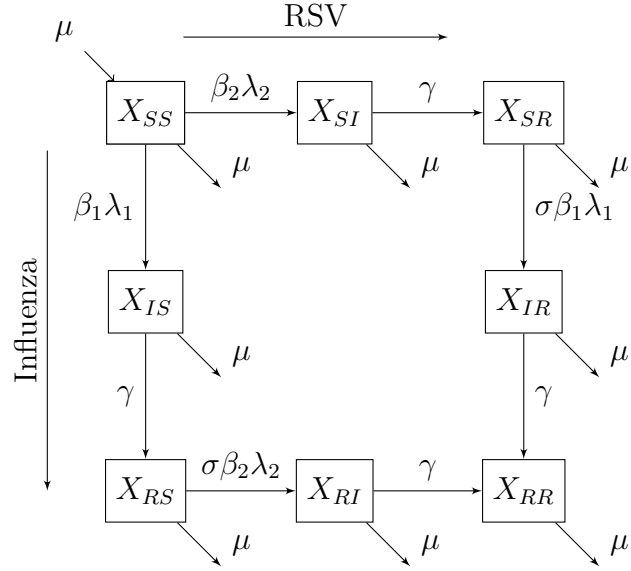


Figure 1: SIR model with two pathogens. X_{kl} represents the number of individuals in immunological status k for pathogen 1 and status l for pathogen 2. Labels above the arrows represent the reaction rates for each reaction type.

and defer the task of defining more complex transition models to future work. Reactions associated with the transition events are illustrated graphically in Figure 1. In our model, the constants β_1 and β_2 represent the contact transmission rate, which describes the flow of individuals from the susceptible group to a group infected with pathogen 1 and 2 respectively. In the context of ARI, the average recovery time is known to be relatively stable and lasts for approximately 7 days (Center for Disease Control and Prevention 2017). Therefore, the rate, γ , at which infected individuals recover (move from infected to temporary immunity in the recovered category) is $1/7 \text{ days}^{-1}$. Since the population is relatively stable over the years under study, we set the birth rate equal to the death rate μ in our transition model. We also assume an average life expectancy of $1/\mu = 70 \text{ years}^{-1}$ (World Health Organization 2017). Constants λ_1 and λ_2 represent the average population infected with pathogens 1 and 2 respectively. Finally, to describe the interaction between influenza and RSV, we use the cross-immunity or cross-enhancement parameter σ . Cross-immunity is present when $0 < \sigma < 1$, indicating that the presence of one pathogen inhibits the presence of the other. A value of $\sigma = 0$ confers complete protection against secondary infection; a value of $\sigma = 1$ confers no protection; and a value of $\sigma > 1$ represents increasing degree of cross-enhancement, indicating that the presence of one pathogen enhances the presence of the other (Adams and Boots 2007).

We next make the following standard assumptions on the infection states X . Transitions from one state to another depend only on the time interval but not on absolute time, mathematically, $X(\Delta t)$ and $X(t + \Delta t) - X(t)$ are identically distributed. Additionally,

Table 1: Description of two-pathogen SIR model parameters

Parameter	Description
Ω	Average yearly population size (known and assumed stable over time)
σ	Cross-immunity or enhancement
λ_p	Proportion of individuals infected with pathogen $p = 1, 2$
β_p	Baseline transmission rate for pathogen $p = 1, 2$
μ	Birth and death rate: $1/70 \text{ years}^{-1}$
γ	Recovery rate: $365/7 \text{ years}^{-1}$

the probability of two or more transitions occurring simultaneously is assumed to be zero. Since the model preserves mass, the constraint $\Omega = X_{SS} + X_{IS} + X_{SR} + X_{RS} + X_{SI} + X_{RR} + X_{RI} + X_{IR}$ is satisfied. The probability mass function p_t describing the probability of being in state $X = x$ at time t evolves according to the Kolmogorov forward equation (chemical master equation, or CME),

$$\frac{dp_t(x)}{dt} = \sum_{j=1}^{\mathcal{R}} \{a_j(x - v_j)p_t(x - v_j) - a_j(x)p_t(x)\}, \quad (1)$$

where the transition probabilities $a_j(x)$ are obtained by multiplying the rates shown in Figure 1 by Δt sufficiently small (Gillespie 2007; Allen 2008), and $v_j(t)$ are stoichiometric vectors whose elements in $\{-1, 0, 1\}$ describe the addition or subtraction of mass from a particular compartment. A list with the \mathcal{R} reactions and the explicit form of these terms are defined in the supplementary material. The large-volume approximation to this system characterizes the distribution of the Markov process $X(t), t \in [0, T]$ as,

$$X(t) \mid \theta \sim \mathcal{N} \left(\Omega \phi(t) + \Omega^{1/2} \tilde{\xi}(t), \Omega C(t, t) \right), \quad t \in [0, T]. \quad (2)$$

The next section defines the quantities $\phi, \tilde{\xi}, C$, and explains the above large volume approximation. Readers who are not interested in the details of the approximation may skip this section. Section 3.3 describes how this approximation is used to model aggregated report data.

3.2 Recovering Model Components via Linear Noise Approximation

A large-volume approximation of the CME (1) is given by the van Kampen expansion, which can then be computed via the Linear Noise Approximation (LNA) (Van Kampen 1992). For large Ω the system states X can be expressed as the sum of a deterministic term $\phi : [0, T] \rightarrow \mathbb{R}^{+\mathcal{S}}$ and a stochastic term ξ ,

$$X(t) = \Omega\phi(t) + \Omega^{1/2}\xi(t), \quad t \in [0, T]. \quad (3)$$

Assuming constant average concentration, the size of the stochastic component will increase as the square root of population size.

Let $S = [v_1, \dots, v_{\mathcal{R}}]$ be a $\dim\{X(t)\} \times \mathcal{R}$ stoichiometric matrix that describes changes in the population size due to each of the \mathcal{R} reactions. The time-evolution of the term of order $\Omega^{1/2}$ (Van Kampen 1992), $\phi_i(t) = \lim_{\Omega, X \rightarrow \infty} X_i(t)/\Omega$ is governed by the ODE initial value problem,

$$\begin{cases} \frac{d\phi_i(t)}{dt} = \sum_{j=1}^{\mathcal{R}} S_{ij}a_j(\phi(t)), & t \in (0, T], \quad i = 1, \dots, \dim\{X(t)\}, \\ \phi_i(0) = \phi_0, & i = 1, \dots, \dim\{X(t)\}. \end{cases} \quad (4)$$

Following the assumption in (Golightly et al. 2012), we take $\phi_0 = X(0)/\Omega$.

The stochastic process ξ is governed by the Itô diffusion equation,

$$d\xi(t) = A(t)\xi(t)dt + \sqrt{B(t)}dW(t), \quad t \in [0, T], \quad (5)$$

where $A(t) = \frac{\partial S a(\phi(t))}{\partial \phi(t)}$, $B(t) = S \text{diag}\{a(\phi(t))\} S^\top$, and $W(t)$ denotes the \mathcal{R} dimensional Wiener process (Van Kampen 1992; Gillespie 2007). For fixed or Gaussian initial conditions, the SDE in (5) can be solved analytically (Golightly et al. 2012). The solution of this equation is a Gaussian process with mean $\tilde{\xi}$ and covariance C (Van Kampen 1992), that is,

$$\xi(t) \sim \mathcal{N}(\tilde{\xi}(t), C(t, t)), \quad t \in [0, T], \quad (6)$$

where $\tilde{\xi}(t)$ and $C(t, t)$ are obtained (see Van Kampen (1992), pp. 210-214) by solving the ODE initial value problem,

$$\begin{cases} \frac{\partial \tilde{\xi}(t)}{\partial t} = \Phi(t)\tilde{\xi}(t_0), & t \in (0, T], \\ \tilde{\xi}(0) = \tilde{\xi}_{t_0}, \end{cases} \quad (7)$$

where $\Phi(t)$ is the evolution, or fundamental matrix (Grimshaw 1991) determined by the matrix equation,

$$\begin{cases} \dot{\Phi}(t) = A(t)\Phi(t), & t \in (0, T], \\ \Phi(0) = I. \end{cases} \quad (8)$$

The covariance C is obtained by solving,

$$\begin{cases} \frac{dC(t)}{dt} = C(t)A(t)^T + A(t)C(t) + B(t)C(t), & t \in (0, T], \\ C(0) = C_0. \end{cases} \quad (9)$$

It follows from (3) and (6) that the transition densities of $X(t)$ are given by (2).

3.3 Probability Model for Epidemic Data From two Sources

In this analysis we take a Bayesian inferential approach where estimation and uncertainty quantification are based on functionals of the posterior distribution of unknown model parameters conditional on available data. In particular, interest lies in the posterior distribution of the vector of model parameters,

$$\theta = [\beta_1, \beta_2, \sigma, x(0)], \quad (10)$$

defined in Section 3.1, augmented with unknown initial conditions for X , conditional on epidemic data from two sources, described below.

Our first data set consists of indirect observations of the Markov process $X(t) : t \in [0, T]$. Let $Z(t) = X_{IS}(t) + X_{IR}(t) + X_{SI}(t) + X_{RI}(t)$ be the total number of reported infections from influenza and RSV. We therefore define this transformation via the vector $G^T = [0, 1, 0, 1, 1, 0, 1, 0]$ to define the desired observation process $Z(t) = G^T X = X_{IS}(t) +$

$X_{IR}(t) + X_{SI}(t) + X_{RI}(t)$. Setting $\tilde{\xi}(0) = 0$, it follows that $\tilde{\xi}(t) = 0$ for all $t \in [0, T]$. Thus,

$$Z(t_i) \mid X(t_i), \theta \sim \mathcal{N}(\Omega G^\top \phi(t_i), \Omega G^\top C(t_i, t_i) G), \quad i = 1, \dots, N. \quad (11)$$

Note that for this analysis we have chosen to use the Linear Noise Approximation directly to define a Normal model of reported aggregated ARI cases. The main reason for this simplification is computational (Golightly et al. 2015), since the resulting posterior distribution over the states has closed form Kalman updates which are exploited to significantly speed up the inferential procedure. An alternative modeling approach would define, for example, a Poisson model for the count data with the mean given by the observation process Z . The resulting posterior distribution over the states will not be available in closed form, and an additional layer of sampling would be required at each observation location for each Markov chain Monte Carlo (MCMC) iteration used. We reserve computational implementation of this extension for future work.

The aggregate number of ARI cases in the San Luis Potosí data also includes infections by viruses other than influenza and RSV. Although these may be responsible for a significant fraction of all ARI cases, influenza and RSV are the two viruses that drive the epidemic fluctuations observed during the winter outbreaks in each year. Therefore, we will include other viruses in the model as a background term. We will assume a constant background, α , and assume that a fixed proportion, r , of all individuals infected with ARI seek consultation. Therefore, considering the Normal model justified above, we have the likelihood of the

Table 2: Description of initial conditions and error model parameters

Parameter	Description
α	Reported infections from ARI other than influenza or RSV
Σ	Error variance
r	Reporting proportion for those infected with an ARI

observed aggregated reports,

$$Y(t_i) \mid Z(t_i), X(t_i), \theta, \tau \sim \mathcal{N} \left(rZ(t_i, \theta) + r\alpha, r^2\Omega G^T C G + \Sigma \right), \quad i = 1, \dots, N, \quad (12)$$

where Σ represents the error variance and the vector of auxiliary parameters defining the error model is,

$$\tau = [\alpha, \Sigma, r].$$

Additional data described in Section 2 is incorporated into the model to identify the dynamics of separate pathogens, which cannot be recovered by only observing aggregate infections Y . Samples of size $n(t_j)$, of infants younger than 5 years of age were tested for influenza and RSV at times $t_j, j = 1, \dots, M$ in each year. We assume that the pathogen type is identified without error and that the proportion of influenza infections among infants is representative of that in the general population. Let $T(t_j)$ represent the number of infants that were diagnosed with influenza out of a sample of $n(t_j)$ infants. The likelihood for this

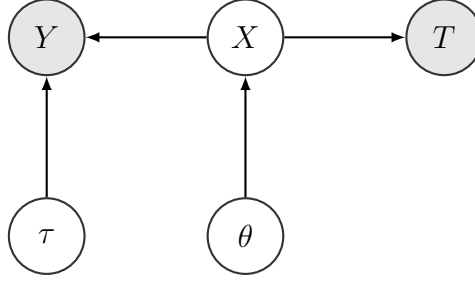


Figure 2: Directed acyclic graph diagram for the data error model; arrows represent conditional dependence; nodes shaded in gray indicate observed data.

data is,

$$T(t_j) \mid X(t_j), n(t_j), \theta \sim \text{Bin}(n(t_j), p(t_j)), \quad j = 1, \dots, M, \quad (13)$$

where $p(t_j) = \{X_{IS}(t_j) + X_{IR}(t_j)\} / \{X_{IS}(t_j) + X_{IR}(t_j) + X_{SI}(t_j) + X_{RI}(t_j)\}$ is computed from the states predicted by the mathematical model at time t_j under model parameters θ .

3.4 Prior Probability Models for Unknown Components

Prior distributions on the model and auxiliary parameters are obtained by expert elicitation and based on the following facts. As discussed in section (3), the cross-immunity or cross-enhancement parameter σ is necessarily bounded below by 0. To enforce this lower bound, we choose a Gamma prior distribution. Transmission rate $\beta_p, p = 1, 2$, is related to the unknown reproductive number R_{p0} for each virus, which takes values between 1 and 3 (Biggerstaff et al. 2014), by the expression $\beta_p = R_{p0}(\gamma + \mu)$ (Van den Driessche

and Watmough 2002). Equation (4) is normalized, so the elements of $X(0)/\Omega$ lie on the simplex, which suggests a prior Beta distribution with a restriction that the sum of the elements of $X(0)/\Omega$ should be equal 1. Initially, we expect nearly the entire population to be susceptible ($X_{SS}(0)/\Omega \approx 1$) and the number of infected individuals to be close to zero ($X_{I.}(0), X_{.I}(0) \approx 0$), which suggests placing Beta priors on the initial states. Similarly, the parameter r is a proportion, and α/Ω is the background scaled to lie between 0 and 1. Finally, Σ is positive, and we choose Gamma prior parameters to yield a relatively flat density reflecting our lack of prior knowledge about this constant outside of the positivity constraint. Prior specifications for all model and auxiliary parameters are provided below. The index $p = 1, 2$ represents influenza and RSV respectively, and $\{\bullet\} = S, R$ represents either the susceptible or recovered state.

$$\begin{array}{lll}
\beta_p \sim \mathcal{G}(20, 3), \ p = 1, 2 & X_{SS}(0)/\Omega \sim B(10, 2) & \mathbf{1}^\top \cdot X(0) = \Omega \\
\sigma \sim \mathcal{G}(4, 1/5) & X_{I.}(0)/\Omega \sim B(a_1, b_1) & E[X_{I.}(0)] = \Omega \times 10^{-5} \\
\alpha/\Omega \sim B(2, 100) & X_{.I}(0)/\Omega \sim B(a_2, b_2) & E[X_{.I}(0)] = 2\Omega \times 10^{-5} \\
\Sigma \sim \mathcal{G}(1, 1/50) & X_{RS}(0)/\Omega \sim B(a_3, b_3) & E[X_{RS}(0)] = 0.016\Omega \\
r \sim B(10, 2) & X_{SR}(0)/\Omega \sim B(a_3, b_3) & E[X_{SR}(0)] = 0.016\Omega.
\end{array}$$

3.5 Posterior Probability of Model Components

The product of the prior probability densities and conditional densities (12), (13), (2) is proportional to the posterior distribution,

$$\theta, \tau, X(t) \mid \{Y(t_i)\}_{i=1, \dots, N}, \{T(t_j), n(t_j)\}_{j=1, \dots, M}, \quad (14)$$

which can then be marginalized over the auxiliary parameters τ . In the supplementary material we describe the Parallel Tempering Markov chain Monte Carlo (PTMCMC, Geyer 1991) algorithm implementing the Particle Marginal Metropolis-Hastings (PMMC, Golightly et al. 2015) scheme, used to obtain approximate samples from the marginal posterior distribution over θ .

4 RESULTS

This section first describes results of a simulation conducted to assess the feasibility of our approach and to study the impact of posterior uncertainty and the qualitative behavior of posterior sample paths when unknown initial conditions are included in the model. We then analyze six years of data from San Luis Potosí, México with the goal of separately identifying the dynamics of influenza and RSV.

Our analysis was performed using Python. Python module “corner” (Foreman-Mackey 2016) was used to display bivariate posterior correlation plots and module “pymc3” (Salvatier J 2016) was used to compute pointwise highest posterior density intervals (HPD).

4.1 Inference Based on Simulated Data

A simulation study was conducted to assess the performance of our inferential approach. Data were simulated by first generating a sample path $X(t)$ from the solution of equation (1) with parameters set to a-priori reasonable values discussed in Section 3.4, and a population

size of $\Omega = 2.5 \times 10^6$, comparable to the total population in our motivating problem. A forward simulation was conducted using the Gillespie algorithm (Thanh and Priami 2015), an asymptotically exact, but computationally expensive technique. Observed states for each pathogen were then used to simulate the data $Y(t_i), T(t_i), i = 1, \dots, 52$ following the observation models (12) and (13). The observation transformation for Y consisted of aggregated influenza and RSV reports in addition to a background of $\alpha = 2.0 \times 10^4$ infections with error variance $\Sigma = 2.5 \times 10^7$. For the estimation, we rescaled the states by $1/\Omega$ to obtain $\alpha/\Omega = 8.0 \times 10^{-3}$ and $\Sigma/\Omega^2 = 4.0 \times 10^{-6}$ to match the scale of the other parameters of interest. The small simulated samples of ARI infections, T , which correctly identified the pathogen type, were chosen to be comparable in size to the data. We conducted 7.0×10^5 MCMC iterations, of which 3.5×10^5 were discarded as burn-in after performing convergence diagnostics.

We analyzed two scenarios. First, we assumed a simplification in which initial conditions were known exactly and inferred the remaining parameters. The top panels of Figure 4 and Table 3 summarize the results and compare them to the ground truth. We then assumed a more realistic scenario in which initial conditions, model parameters, and auxiliary parameters were all unknown. The lower panel of Figure 3 and Table 3 summarize these results. Our results are in agreement with Shrestha et al. (2011), who note that the precision of the estimates typically increases when the initial conditions are known. Our simulation results show that while uncertainty in the initial conditions increases posterior variance in the remaining parameters, the predicted qualitative behavior of the disease dynamics does

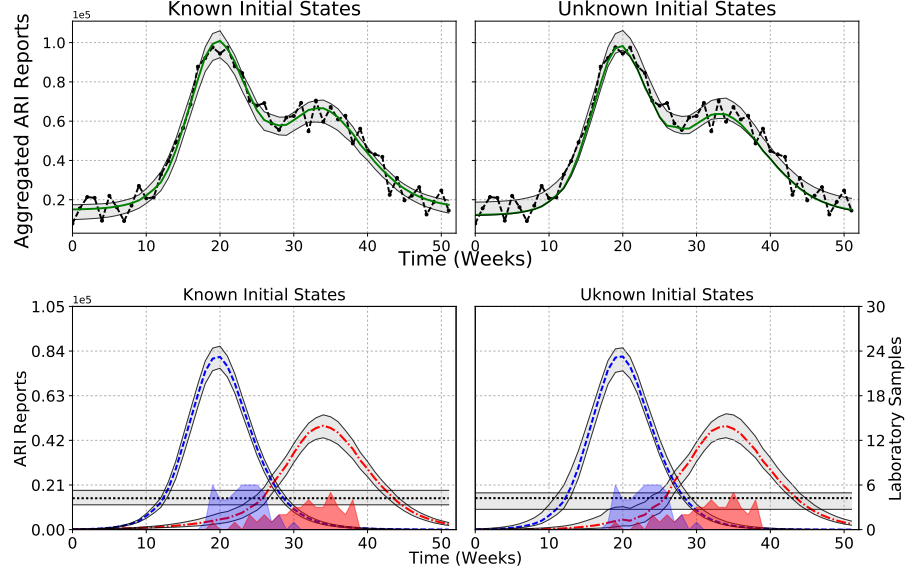


Figure 3: Comparison of simulation scenario 1 (known initial states, left column) and scenario 2 (unknown initial states, right column). The top row shows the aggregated maximum a posteriori (MAP) estimate (solid green line) and 95% HPD intervals for the aggregated ARI reports (solid black lines). The bottom row shows disaggregated MAP estimates for influenza, RSV, background infections (dotted red, blue, and black lines, respectively), and their respective 95% HPD intervals (solid black lines).

not change. Importantly, in both cases, we can identify the dynamics of each pathogen independently.

Table 3: Simulation results assuming known and unknown initial conditions

Scenario 1: known initial states			
Parameter	Simulation value	MAP estimate	95% HPD interval
β_1	67	66.97	(65.97, 69.95)
β_2	79.5	80.44	(79.32, 81.80)
σ	1.30	1.30	(1.18, 1.35)
α/Ω	8.00×10^{-3}	0.01	$(5.95 \times 10^{-3}, 9.42 \times 10^{-3})$
Σ/Ω^2	4.00×10^{-6}	3.73×10^{-6}	$(2.84 \times 10^{-6}, 6.22 \times 10^{-6})$
r	0.80	0.78	(0.72 , 0.84)
Scenario 2: unknown initial states			
Parameter	Simulation value	MAP estimate	95% HPD interval
β_1	67.00	69.22	(63.89, 84.69)
β_2	79.50	76.53	(72.60, 90.39)
σ	1.30	1.00	(0.85, 1.23)
α/Ω	8.00×10^{-3}	0.01	$(5.10 \times 10^{-3}, 9.20 \times 10^{-3})$
Σ/Ω^2	4.00×10^{-6}	3.69×10^{-6}	$(2.66 \times 10^{-6}, 6.18 \times 10^{-6})$
r	0.80	0.75	(0.70, 0.94)
X_{SS}	0.85	0.94	(0.79, 0.97)
X_{IS}	5.22×10^{-5}	5.15×10^{-6}	$(1.78 \times 10^{-9}, 2.28 \times 10^{-5})$
X_{RS}	4.32×10^{-2}	0.01	$(4.21 \times 10^{-3}, 3.0 \times 10^{-2})$
X_{SI}	1.63×10^{-5}	1.13×10^{-5}	$(2.4 \times 10^{-9}, 9.79 \times 10^{-5})$
X_{RI}	4.16×10^{-5}	4.86×10^{-5}	$(9.69 \times 10^{-9}, 9.47 \times 10^{-5})$
X_{SR}	3.80×10^{-2}	1.34×10^{-2}	$(5.60 \times 10^{-3}, 2.40 \times 10^{-2})$
X_{IR}	3.54×10^{-5}	3.66×10^{-6}	$(6.43 \times 10^{-10}, 3.96 \times 10^{-5})$

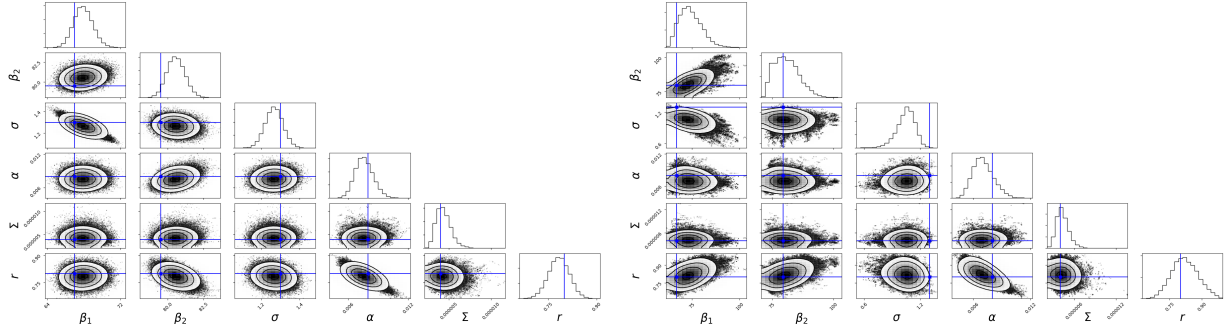


Figure 4: Pairwise marginal posterior plots for the model parameters for simulation scenario 1 (known initial conditions, left panel) and simulation scenario 2 (unknown initial conditions, right panel).

4.2 Inference Based on Data From San Luis Potosí, México

We now turn to the motivating application of separately identifying the dynamics of influenza and RSV from aggregate ARI counts and auxiliary virological testing data from San Luis Potosí, México. Figures 5 and 6 describe the marginal posterior distribution of the aggregated ARI infection trajectories, and the individual disease dynamics of influenza and RSV. Two years in particular exemplify the opportunities and challenges of using auxiliary virological testing data to identify individual pathogens. As an example, in year 2003-04 we are able to identify the two peaks when the auxiliary samples clearly indicate the presences of two different outbreaks. In another example, in year 2006-07 the auxiliary information about the second outbreak is less informative, and thus one of the pathogens is able to explain the entire pattern of the aggregate outbreak. Bayes estimators of the posterior parameters as well as highest posterior density intervals are provided for both these cases in Table 5. In general, larger virological testing samples tend to be more informative, and

more often allow the identification of individual disease dynamics when the epidemic peaks occur relatively far apart.

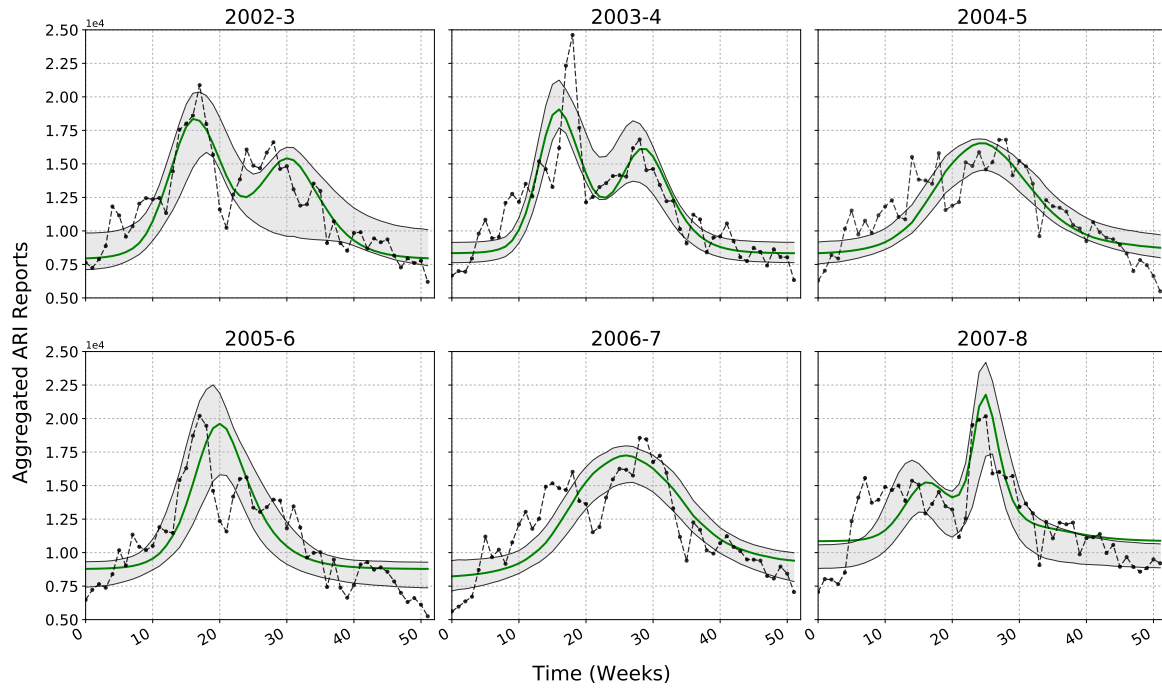


Figure 5: Aggregated ARI reports from San Luis Potosí, México (dotted black line) measured from August to July of the following year. Maximum a posteriori estimate of aggregated ARI reports and 95% highest posterior density intervals are shown in green and solid black lines respectively.

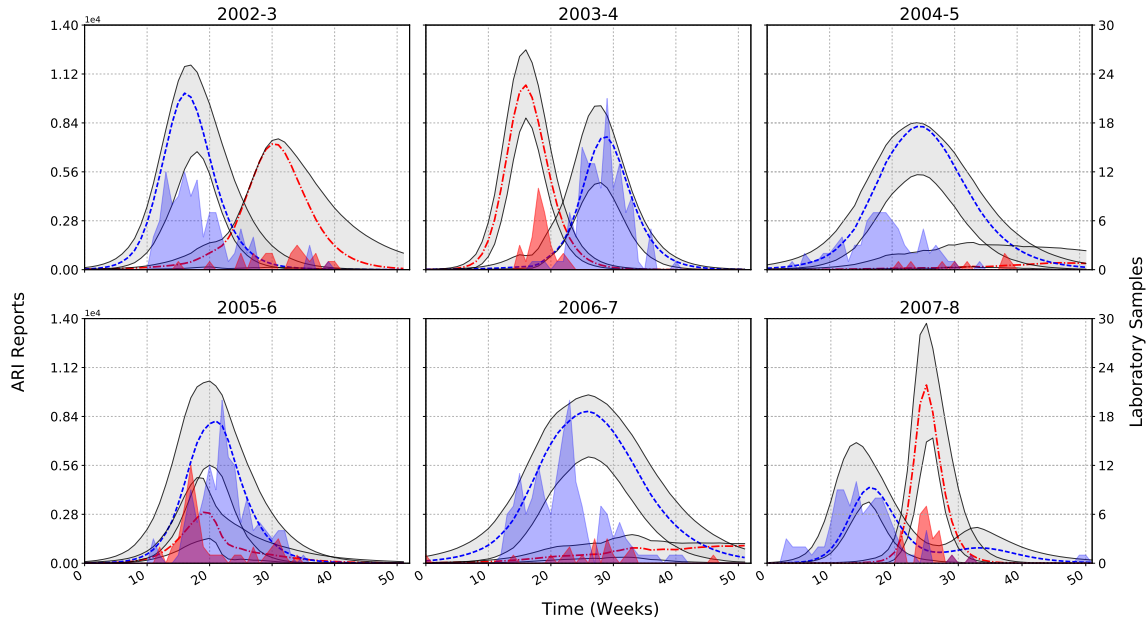


Figure 6: Left axis: Maximum a posteriori estimate of influenza (red dashed line) and RSV (blue dotted line) reports and their respective 95% highest posterior density intervals (solid black lines). Right axis: Reports of influenza and RSV from random samples of children under 5 years of age at Hospital Central “Dr. Ignacio Morones Prieto” (light and dark gray patches respectively).

Table 4: Posterior summaries for the analysis in year 2003-04

Parameter	MAP	95% HPD	Parameter	MAP	95% HPD
β_1	87.86	(82.21, 111.28)	X_{SS}	0.92	(0.63, 1.00)
β_2	73.05	(68.31, 94.23)	X_{IS}	5.51×10^{-6}	$(1.26 \times 10^{-10}, 4.05 \times 10^{-5})$
σ	1.19	(0.47, 1.38)	X_{RS}	1.37×10^{-2}	$(0.43, 3.57) \times 10^{-2}$
α/Ω	5.70×10^{-2}	$(3.50, 6.60) \times 10^{-2}$	X_{SI}	1.44×10^{-5}	$(2.94 \times 10^{-9}, 2.49 \times 10^{-4})$
Σ/Ω^2	5.58×10^{-7}	$(4.42, 0.10) \times 10^{-7}$	X_{RI}	6.24×10^{-6}	$(5.51 \times 10^{-9}, 2.45 \times 10^{-4})$
r	5.95×10^{-2}	$(5.20, 8.60) \times 10^{-2}$	X_{SR}	1.59×10^{-2}	$(0.28, 3.16) \times 10^{-2}$
			X_{IR}	7.61×10^{-6}	$(6.38 \times 10^{-10}, 6.48 \times 10^{-5})$

Table 5: Posterior summaries for the analysis in year 2006-07

Parameter	MAP	95% HPD	Parameter	MAP	95% HPD
β_1	74.26	(62.62, 99.95)	X_{SS}	0.85	(0.59, 0.95)
β_2	74.67	(64.50, 101.57)	X_{IS}	1.617e-07	(2.31 $\times 10^{-10}$, 3.58 $\times 10^{-5}$)
σ	0.379	(0.09, 0.84)	X_{RS}	0.01	(0.005, 0.03)
α/Ω	0.016	(0.004, 0.02)	X_{SI}	6.23×10^{-5}	$(2.35 \times 10^{-10}, 2.36 \times 10^{-4})$
Σ/Ω^2	7.075×10^{-7}	(4.05, 9.9) $\times 10^{-7}$	X_{RI}	4.21×10^{-5}	$(3.21 \times 10^{-9}, 1.69 \times 10^{-4})$
r	2.12×10^{-1}	(0.14, 0.52)	X_{SR}	0.02	(0.003, 0.03)
			X_{IR}	8.43×10^{-6}	$(8.94 \times 10^{-7}, 3.23 \times 10^{-5})$

5 DISCUSSION

We have presented a Bayesian hierarchical modeling approach for identifying individual disease dynamics defined by a SIR model for the temporal evolution and interaction of two distinct pathogens in a large population. Our model enforces both hard physical constraints associated with the mathematical model and soft constraints related to prior expert knowledge which can aid inference in data-poor scenarios. Results are obtained in the realistic setting where ARI-causing pathogens cannot be identified based on symptoms alone, and only aggregate counts of infections are available.

Though the mathematical model is only partially symmetric, the availability of only aggregated reports leads to the problem of practical identifiability for individual dynamics and associated rate constants. We resolve this by including in the model auxiliary data from a small sample of patients who underwent virological testing to identify the ARI-causing pathogen. We show that collecting even a moderate number of such extra observations, as was done in Hospital Central “Dr. Ignacio Morones Prieto” in San Luis Potosí, México, can allow the identification of distinct pathogen dynamics, thus aiding in the goal of planning and public health administration at a relatively small additional cost. Qualitatively, our results indicate that detection of individual dynamics can be achieved with a smaller sample when the peak circulation of the epidemics is far apart, as in the year 2003-04. When ARI caused by both pathogens peak in close proximity, as in the year 2006-07, more laboratory data is required to correctly identify them.

These results can be of great use in epidemiological analyses that are carried out to estimate the burden of influenza on morbidity and mortality at local, national, or regional levels. Most current estimates of influenza-associated morbidity and mortality do not take into account the contribution of respiratory syncytial virus to excess mortality, due mainly to the paucity of virological surveillance information for all relevant viruses to incorporate in these analysis. As such, the results of this study indicate that the availability of a relatively small number of weekly influenza and respiratory syncytial virus detections would be sufficient to establish the seasonal behavior of these agents and to ultimately estimate the burden of disease associated with each.

In future work we plan to consider more realistically complex mathematical models by accounting for vaccination effects and seasonal forcing. Resolving the identifiability constraints with these additional model components will require the use of other sources of data, such as vaccination reports and local climate variables. Another reasonable assumption is that yearly outbreaks are related to one another through dependence on the rate parameters defining the mathematical model. Dependence between seasonal outbreaks can be incorporated in the model by inferring each year's outbreak simultaneously. Borrowing information between years in this way may help to alleviate some problems with identifiability but at a higher computational cost.

References

- Adams, B. and Boots, M. (2007). “The Influence of Immune Cross-Reaction on Phase Structure in Resonant Solutions of a Multi-Strain Seasonal SIR Model”. *Journal of theoretical biology*, 248(1):202–211.
- Allen, L. J. (2008). “An Introduction to Stochastic Epidemic Models”. In *Mathematical epidemiology*, pages 81–130. Springer.
- Ånestad, G. (1987). “Surveillance of Respiratory Viral Infections by Rapid Immunofluorescence Diagnosis, with Emphasis on Virus Interference”. *Epidemiology and infection*, 99(02):523–531.
- Anestad, G. et al. (1982). “Interference Between Outbreaks of Respiratory Syncytial Virus and Influenza Virus Infection”. *Interference between outbreaks of respiratory syncytial virus and influenza virus infection.*, 1.
- Anestad, G. and Nordbo, S. (2009). “Interference Between Outbreaks of Respiratory Viruses”. *Euro Surveill*, 14(41):19359.
- Ávila Adarne, L. and Castellanos, J. (2013). “Diagnóstico Viroológico de la Infección por Virus Sincicial Respiratorio”. *Revista de Salud Bosque*, 3(1):23–36.
- Biggerstaff, M., Cauchemez, S., Reed, C., Gambhir, M., and Finelli, L. (2014). “Estimates of the Reproduction Number for Seasonal, Pandemic, and Zoonotic Influenza: a Systematic Review of the Literature”. *BMC infectious diseases*, 14(1):480.

- Bloom-Feshbach, K., Alonso, W. J., Charu, V., Tamerius, J., Simonsen, L., Miller, M. A., and Viboud, C. (2013). “Latitudinal Variations in Seasonal Activity of Influenza and Respiratory Syncytial Virus (RSV): a Global Comparative Review”. *PloS one*, 8(2):e54445.
- Center for Disease Control and Prevention (2017). [online] “Clinical Signs and Symptoms of Influenza”. <https://www.cdc.gov/flu/professionals/acip/clinical.htm>.
- Chan, K. P., Wong, C. M., Chiu, S. S., Chan, K. H., Wang, X. L., Chan, E. L., Peiris, J. M., and Yang, L. (2014). “A Robust Parameter Estimation Method for Estimating Disease Burden of Respiratory Viruses”. *PloS one*, 9(3):e90126.
- Chaw, L., Kamigaki, T., Burmaa, A., Urtnasan, C., Od, I., Nyamaa, G., Nymadawa, P., and Oshitani, H. (2016). “Burden of Influenza and Respiratory Syncytial Virus Infection in Pregnant Women and Infants Under 6 Months in Mongolia: A Prospective Cohort Study”. *PloS one*, 11(2):e0148421.
- Dukic, V., Lopes, H. F., and Polson, N. G. (2012). “Tracking Epidemics With Google Flu Trends Data and a State-Space SEIR Model”. *Journal of the American Statistical Association*, 107(500):1410–1426.
- Farah, M., Birrell, P., Conti, S., and Angelis, D. D. (2014). Bayesian emulation and calibration of a dynamic epidemic model for A/H1N1 Influenza. *Journal of the American Statistical Association*, 109(508):1398–1411.

- Foreman-Mackey, D. (2016). “corner.py: Scatterplot Matrices in Python”. *The Journal of Open Source Software*, 1(2).
- Geyer, C. (1991). Markov chain Monte Carlo maximum likelihood. In *Computing Science and Statistics, Proceedings of the 23rd Symposium on the Interface*, 156. American Statistical Association.
- Gillespie, D. T. (2007). “Stochastic Simulation of Chemical Kinetics”. *Annu. Rev. Phys. Chem.*, 58:35–55.
- Golightly, A., Henderson, D. A., and Sherlock, C. (2012). “Efficient Particle MCMC for Exact Inference in Stochastic Biochemical Network Models through approximation of expensive likelihoods”.
- Golightly, A., Henderson, D. A., and Sherlock, C. (2015). “Delayed Acceptance Particle MCMC for Exact Inference in Stochastic Kinetic Models”. *Statistics and Computing*, 25(5):1039–1055.
- Golightly, A. and Wilkinson, D. J. (2011). “Bayesian Parameter Inference for Stochastic Biochemical Network Models Using Particle Markov Chain Monte Carlo”. *Interface Focus*.
- Grimshaw, R. (1991). *“Nonlinear Ordinary Differential Equations”*, volume 2. CRC Press.
- Huppert, A. and Katriel, G. (2013). “Mathematical Modelling and Prediction in Infectious Disease Epidemiology”. *Clinical Microbiology and Infection*, 19(11):999–1005.

- Kamo, M. and Sasaki, A. (2002). “The Effect of Cross-Immunity and Seasonal Forcing in a Multi-Strain Epidemic Model”. *Physica D: Nonlinear Phenomena*, 165(3):228–241.
- Komorowski, M., Finkenstädt, B., Harper, C. V., and Rand, D. A. (2009). “Bayesian Inference of Biochemical Kinetic Parameters Using the Linear Noise Approximation”. *BMC bioinformatics*, 10(1):1.
- Kuri-Morales, P., Galván, F., Cravioto, P., Rosas, L. A. Z., and Tapia-Conyer, R. (2006). “Mortalidad en México por Influenza y Neumonía (1990-2005)”. *Salud pública de México*, 48(5):379–384.
- Mangtani, P., Hajat, S., Kovats, S., Wilkinson, P., and Armstrong, B. (2006). “The Association of Respiratory Syncytial Virus Infection and Influenza with Emergency Admissions for Respiratory Disease in London: an Analysis of Routine Surveillance Data”. *Clinical infectious diseases*, 42(5):640–646.
- Modjarrad, K., Giersing, B., Kaslow, D. C., Smith, P. G., Moorthy, V. S., et al. (2016). “WHO Consultation on Respiratory Syncytial Virus Vaccine Development Report From a World Health Organization Meeting Held on 23–24 March 2015”. *Vaccine*, 34(2):190–197.
- Salvatier J, Wiecki TV, F. C. (2016). [online] “Probabilistic Programming in Python using PyMC3. PeerJ Computer science 2:e55”.
- Shrestha, S., King, A. A., and Rohani, P. (2011). “Statistical Inference for Multi-Pathogen Systems”. *PLoS Comput Biol*, 7(8):e1002135.

- Siettos, C. I. and Russo, L. (2013). “Mathematical Modeling of Infectious Disease Dynamics”. *Virulence*, 4(4):295–306.
- Star, L. and Moghadas, S. (2010). “The Role of Mathematical Modelling in Public Health Planning and Decision Making”. *Purple Paper. National Collaborative Center for Infectious Diseases. Issue*, (22).
- Thanh, V. H. and Priami, C. (2015). “Simulation of Biochemical Reactions with Time-Dependent Rates by the Rejection-Based Algorithm”. *The Journal of chemical physics*, 143(5):08B601.1.
- Thomas, P., Matuschek, H., and Grima, R. (2012). “Intrinsic Noise Analyzer: a Software Package for the Exploration of Stochastic Biochemical Kinetics Using the System Size Expansion”. *PloS one*, 7(6):e38518.
- Thompson, W. W., Shay, D. K., Weintraub, E., Brammer, L., Cox, N., Anderson, L. J., and Fukuda, K. (2003). “Mortality Associated with Influenza and Respiratory Syncytial Virus in the United States”. *Jama*, 289(2):179–186.
- Van den Driessche, P. and Watmough, J. (2002). “Reproduction Numbers and Sub-Threshold Endemic Equilibria for Compartmental Models of Disease Transmission”. *Mathematical biosciences*, 180(1):29–48.
- Van Kampen, N. G. (1992). “*Stochastic Processes in Physics and Chemistry*”, volume 1. Elsevier.

- Vasco, D. A., Wearing, H. J., and Rohani, P. (2007). “Tracking the Dynamics of Pathogen Interactions: Modeling Ecological and Immune-Mediated Processes in a Two-Pathogen Single-Host System”. *Journal of Theoretical Biology*, 245(1):9–25.
- Velasco-Hernández, J. X., Núñez-López, M., Comas-García, A., Cherpitel, D. E. N., and Ocampo, M. C. (2015). “Superinfection Between Influenza and RSV Alternating Patterns in San Luis Potosí State, México”. *PloS one*, 10(3):e0115674.
- Wilkinson, D. (2006). “*Stochastic Modelling for Systems Biology*”. Chapman & Hall/CRC Mathematical & Computational Biology. Taylor & Francis.
- Wilkinson, D. (2011). “*Stochastic Modelling for Systems Biology, Second Edition*”. Chapman & Hall/CRC Mathematical and Computational Biology. Taylor & Francis.
- World Health Organization (2017). [online] “Life Expectancy”. http://www.who.int/gho/mortality_burden_disease/life_tables/situation_trends/en/.

Supplementary Material: Identifying Individual Disease Dynamics in a Stochastic Multi-pathogen Model From Aggregated Reports and Laboratory Data

Yury E. García, Oksana A. Chkrebtii, Marcos A. Capistrán,
Daniel E. Noyola

July 19, 2022

1 MODEL

This section provides mathematical details for the two-pathogen SIR model considered in the paper “Identifying Individual Disease Dynamics in a Stochastic Multi-pathogen Model from Aggregated Reports and Laboratory Data” by García et al., including reactions and matrices used to compute the master equation. Computational and algorithmic details are provided in the following section.

Table 1: All possible reactions in the system; v_i is the stoichiometric vector, and $a_i(x)$ is the reaction rate for the i th reaction, $i = 1, \dots, 17$.

Reactions	Propensity	Stoichiometric vector
$\mu \rightarrow X_{SS}$	$a_1(x) = \mu\Omega + o(\Delta t)$	$v_1 = [1, 0, 0, 0, 0, 0, 0, 0]$
$X_{SS} \rightarrow X_{SI}$	$a_2(x) = \beta_2\lambda_2x_{ss} + o(\Delta t)$	$v_2 = [-1, 0, 0, 1, 0, 0, 0, 0]$
$X_{SS} \rightarrow X_{IS}$	$a_3(x) = \beta_1\lambda_1x_{ss} + o(\Delta t)$	$v_3 = [-1, 1, 0, 0, 0, 0, 0, 0]$
$X_{SS} \rightarrow \mu$	$a_4(x) = \mu x_{ss} + o(\Delta t)$	$v_4 = [-1, 0, 0, 0, 0, 0, 0, 0]$
$X_{IS} \rightarrow \mu$	$a_5(x) = \mu x_{is} + o(\Delta t)$	$v_5 = [0, -1, 0, 0, 0, 0, 0, 0]$
$X_{IS} \rightarrow X_{RS}$	$a_6(x) = \gamma x_{is} + o(\Delta t)$	$v_6 = [0, -1, 1, 0, 0, 0, 0, 0]$
$X_{RS} \rightarrow \mu$	$a_7(x) = \mu x_{rs} + o(\Delta t)$	$v_7 = [0, 0, -1, 0, 0, 0, 0, 0]$
$X_{RS} \rightarrow X_{RI}$	$a_8(x) = \sigma\beta_2\lambda_2x_{rs} + o(\Delta t)$	$v_8 = [0, 0, -1, 0, 1, 0, 0, 0]$
$X_{SI} \rightarrow X_{SR}$	$a_9(x) = \gamma x_{si} + o(\Delta t)$	$v_9 = [0, 0, 0, -1, 0, 1, 0, 0]$
$X_{SI} \rightarrow \mu$	$a_{10}(x) = \mu x_{si} + o(\Delta t)$	$v_{10} = [0, 0, 0, -1, 0, 0, 0, 0]$
$X_{RI} \rightarrow X_{RR}$	$a_{11}(x) = \gamma x_{ri} + o(\Delta t)$	$v_{11} = [0, 0, 0, 0, -1, 0, 0, 1]$
$X_{RI} \rightarrow \mu$	$a_{12}(x) = \mu x_{ri} + o(\Delta t)$	$v_{12} = [0, 0, 0, 0, -1, 0, 0, 0]$
$X_{SR} \rightarrow \mu$	$a_{13}(x) = \mu x_{sr} + o(\Delta t)$	$v_{13} = [0, 0, 0, 0, 0, -1, 0, 0]$
$X_{SR} \rightarrow X_{IR}$	$a_{14}(x) = \sigma\beta_1\lambda_1x_{sr} + o(\Delta t)$	$v_{14} = [0, 0, 0, 0, 0, -1, 1, 0]$
$X_{IR} \rightarrow \mu$	$a_{15}(x) = \mu x_{ir} + o(\Delta t)$	$v_{15} = [0, 0, 0, 0, 0, 0, -1, 0]$
$X_{IR} \rightarrow X_{RR}$	$a_{16}(x) = \gamma x_{ir} + o(\Delta t)$	$v_{16} = [0, 0, 0, 0, 0, 0, -1, 1]$
$X_{RR} \rightarrow \mu$	$a_{17}(x) = \mu x_{rr} + o(\Delta t)$	$v_{17} = [0, 0, 0, 0, 0, 0, 0, -1]$

1.1 Chemical Master Equation

We define a stochastic SIR model for two pathogens following Kamo and Sasaki (2002).

Let,

$$X(t) = [X_{SS}(t), X_{IS}(t), X_{RS}(t), X_{SI}(t), X_{RI}(t), X_{SR}(t), X_{IR}(t)]^\top,$$

where $X_{kl}(t)$ denotes the number of individuals at time t in immunological status $k \in \{S, I, R\}$ for pathogen 1 (influenza) and immunological status $l \in \{S, I, R\}$ for pathogen 2 (RSV). Vector $x(t)$ corresponds to the realization of the random vector $X(t)$. Reactions associated with these events are listed in Table 1, where $\lambda_1 = (x_{is} + x_{ir})/\Omega$ is the proportion of individuals infected with pathogen 1, and $\lambda_2 = (x_{si} + x_{ri})/\Omega$ is the proportion infected with pathogen 2. The number of possible reaction is $\mathcal{R} = 17$. The evolution of the probability distribution of finding the system in state x at time t is governed by the master equation,

$$\frac{dp_x(t)}{dt} = \sum_{i=1}^{\mathcal{R}} a_i(x - v_i) p_{x-v_i}(t) - \sum_{i=1}^{\mathcal{R}} a_i(x) p_x(t), \quad (1)$$

where v_i is the stoichiometric vector and a_i is the rate of reaction $i = 1, \dots, 17$.

1.2 Large Volume Approximation

The van Kampen expansion (Van Kampen 1992) provides a large volume approximation to the solution of the master equation that is made up of two terms, as follows:

$$X(t) = \Omega\phi(t) + \Omega^{1/2}\xi(t), \quad (2)$$

where $\phi(t)$ describes macroscopic behavior and ξ is the noise term representing the aggregate effects of demographic stochasticity on the system and describing its fluctuations. We make an expansion in the powers of Ω (Van Kampen 1992) and collect powers of $\Omega^{1/2}$ to get the macroscopic law given by the initial value problem,

$$\begin{cases} \frac{d\phi_i(t)}{dt} = \sum_{j=1}^{\mathcal{R}} S_{ij} a_j(\phi(t)), & t \in (0, T], \quad i = 1, \dots, \dim\{X(t)\}, \\ \phi_i(0) = \phi_0, & i = 1, \dots, \dim\{X(t)\}. \end{cases} \quad (3)$$

Here $S = [v_1, \dots, v_{\mathcal{R}}]$ is the stoichiometric matrix and $a(\phi) = [a_1(\phi), \dots, a_{\mathcal{R}}(\phi)]$ is the vector of propensities. The full expressions for the macroscopic equations in the first line of (3) are:

$$\begin{aligned} \frac{d\phi_0(t)}{dt} &= \mu - \beta_2 \lambda_2 \phi_0 - \beta_1 \lambda_1 \phi_0 - \mu \phi_0 - v \phi_0, \\ \frac{d\phi_1(t)}{dt} &= \beta_1 \lambda_1 \phi_0 - \gamma \phi_1 - \mu \phi_1, \\ \frac{d\phi_2(t)}{dt} &= \gamma \phi_1 - \sigma \beta_2 \lambda_2 \phi_2 - \mu \phi_2 + v \phi_0, \\ \frac{d\phi_3(t)}{dt} &= \beta_2 \lambda_2 \phi_0 - \gamma \phi_3 - \mu \phi_3, \\ \frac{d\phi_4(t)}{dt} &= \sigma \beta_2 \lambda_2 \phi_2 - \gamma \phi_4 - \mu \phi_4, \\ \frac{d\phi_5(t)}{dt} &= \gamma \phi_3 - \mu \phi_5 - \sigma \beta_1 \lambda_1 \phi_5, \\ \frac{d\phi_6(t)}{dt} &= -\gamma \phi_6 + \sigma \beta_1 \lambda_1 \phi_5 - \mu \phi_5, \\ \frac{d\phi_7(t)}{dt} &= \gamma \phi_6 + \gamma \phi_4 - \mu \phi_7. \end{aligned} \quad (4)$$

The stochastic process ξ is governed by the Itô diffusion equation,

$$d\xi(t) = A(t)\xi(t)dt + \sqrt{B(t)}dW(t), \quad t \in [0, T], \quad (5)$$

$W(t)$ denotes the \mathcal{R} dimensional Wiener process. Matrix $A(t)$ is given by $A(t) = \frac{\partial S a(\phi(t))}{\partial \phi(t)}$, and matrix $B(t)$ by $B = S \text{diag}(a(\phi)) S^T$ (Van Kampen 1992; Gillespie 2007). Expressions for both matrices are provided in Table 2.

Table 2: Matrices defining the diffusion approximation of the master equation.

$$\begin{bmatrix} -(\beta_2\lambda_2 + \beta_1\lambda_1 + \mu) & -\beta_1\phi_0 & 0 & -\beta_2\phi_0 & 0 \\ 0 & 0 & -\beta_1\phi_0 & 0 & -\beta_2\phi_0 \\ \beta_1\lambda_1 & \beta_1\phi_0 - (\gamma + \mu) & 0 & 0 & 0 \\ \beta_2\lambda_2 & \gamma & -(\beta_2\lambda_2\sigma + \mu) & -\beta_2\phi_2\sigma & -\beta_2\phi_2\sigma \\ 0 & 0 & 0 & \beta_2\phi_0 & 0 \\ 0 & -\beta_1\phi_5\sigma & \beta_2\lambda_2\sigma & \beta_2\sigma\phi_2 - (\gamma + \mu) & 0 \\ 0 & \beta_1\sigma\phi_5 & 0 & 0 & -\beta_1\lambda_1\sigma - \mu \\ 0 & 0 & 0 & \beta_1\lambda_1\sigma & -\beta_1\sigma\phi_5 \\ 0 & 0 & 0 & \gamma & \beta_1\sigma\phi_5 - (\gamma + \mu) \\ & & & & \gamma \\ & & & & -\mu \end{bmatrix}$$

	Matrix B						
$\beta_2\lambda_2\phi_0$	$-\beta_1\phi_0\lambda_1$	0	$-\beta_2\lambda_2\phi_0$	0	0	0	0
$\beta_1\lambda_1\phi_0$							
$(\phi_0+1)\mu$							
$-\beta_1\lambda_1\phi_0$	$\beta_1\lambda_1\phi_0+\phi_1(\gamma+\mu)$	$-\gamma\phi_1$	0	0	0	0	0
0	$-\gamma\phi_1$	$\gamma\phi_1+$					
	$\beta_2\phi_2\lambda_2\sigma+\mu\phi_2$						
$-\beta_2\phi_0\lambda_2$	0	0	$\beta_2\phi_0\lambda_2+\phi_3(\gamma+\mu)$	$-\beta_2\phi_2\lambda_2\sigma$	0	$-\gamma\phi_3$	0
				0			
0	0	$-\beta_2\lambda_2\sigma\phi_2$	$\phi_4(\gamma+\mu)$	$\beta_2\lambda_2\sigma\phi_2$	0	0	$-\gamma\phi_4$
0	0	0	$-\gamma\phi_3$	0	$\gamma\phi_3+\mu\phi_5$	0	
					$\beta_1\lambda_1\sigma\phi_5$	$-\beta_1\phi_5\lambda_1\sigma$	0
0	0	0	0	0	$-\beta_1\sigma\lambda_1\phi_5$	$\beta_1\lambda_1\sigma\phi_5$	
						$(\gamma+\mu)\phi_6$	$-\gamma\phi_6$
0	0	0	0	$-\gamma\phi_4$	0	$-\gamma\phi_6$	$\gamma\phi_4+\gamma\phi_6+\mu\phi_7$

2 COMPUTATION

MCMC samples from the marginal likelihood, $p_{\phi_0}(y|\Theta)$, under LNA are obtained via Parallel Tempering Markov chain Monte Carlo (PTMCMC, Geyer 1991) algorithm implementing the Particle Marginal Metropolis-Hastings (PMMC, Golightly et al. 2015) scheme.

2.1 Simulated Data

For the simulation example, aggregated reports were generated from,

$$AGGdata = r(G^T X + \alpha) + \epsilon,$$

Where $\epsilon \sim \mathcal{N}(0, 2.5 \times 10^7)$ and $\alpha = 2.0 \times 10^5$. For the estimation, we rescaled the states by $1/\Omega$ to obtain $\alpha/\Omega = 8.0 \times 10^{-3}$ and $\Sigma/\Omega^2 = 4.0 \times 10^{-6}$ to match the scale of the other parameters of interest. Laboratory samples were generated by simulating Poisson random variables within a window of two or three weeks before the highest peak of the first outbreak to two or three weeks after the second highest peak as described in the following algorithm.

Algorithm 1: Laboratory Simulated Samples

Result: $INFsample$, $RSVsample$

begin

Take the interval of weeks between 2 weeks before and 2 or 3 weeks after the highest peaks of the two modes (I)

Generate samples equal to the size of I , from a Poisson distribution.

for i in $len(I)$ **do**

$$n = I_i, p = \frac{INFdata_i}{INFdata_i + RSVdata_i}$$

$$INFsample = Bin(n, p)$$

$$RSVsample = |n - INFsample|$$

3 NUMERICAL RESULTS

This section provides posterior summaries and pairwise correlation plots from the analysis of each year considered in this study.

August 2002 - July 2003

Table 3: Posterior summaries for the analysis in year 2002-03

Parameter	MAP	95% HPD	Parameter	MAP	95% HPD
β_1	78.79	(65.55, 100.62)	X_{SS}	0.85	(0.63, 0.96)
β_2	84.65	(72.83, 110.02)	X_{IS}	3.82×10^{-6}	$(1.26 \times 10^{-10}, 4.05 \times 10^{-5})$
σ	1.05	(0.47, 1.38)	X_{RS}	0.02	(0.004, 0.04)
α/Ω	0.04	(0.02, 0.05)	X_{SI}	6.70×10^{-5}	$(2.94 \times 10^{-9}, 2.49 \times 10^{-4})$
Σ/Ω^2	4.85×10^{-7}	$(4.22 \times 10^{-7}, 1.34 \times 10^{-6})$	X_{RI}	7.55×10^{-5}	$(5.51 \times 10^{-9}, 2.45 \times 10^{-4})$
r	0.09	(0.07, 0.16)	X_{SR}	0.01	(0.003, 0.03)
			X_{IR}	6.87×10^{-6}	$(6.38 \times 10^{-10}, 6.48 \times 10^{-5})$

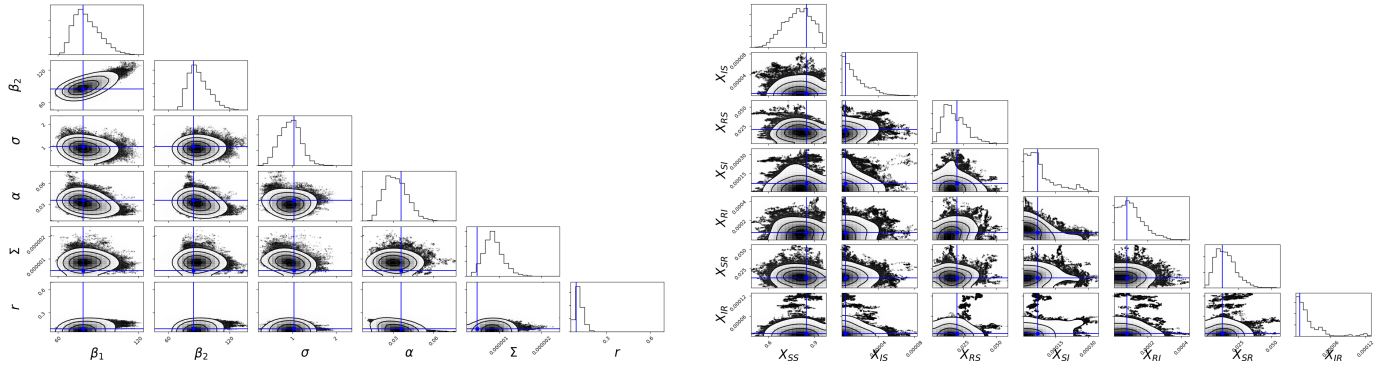


Figure 1: Pairwise marginal posterior plots for the model parameters (top panel) and initial conditions and auxiliary parameters (bottom panel) from the analysis in year 2002-03.

August 2003 - July 2004

Table 4: Posterior summaries for the analysis in year 2003-04

Parameter	MAP	95% HPD	Parameter	MAP	95% HPD
β_1	87.86	(82.21, 111.28)	X_{SS}	0.92	(0.63, 1.00)
β_2	73.05	(68.31, 94.23)	X_{IS}	5.51×10^{-6}	$(1.26 \times 10^{-10}, 4.05 \times 10^{-5})$
σ	1.19	(0.47, 1.38)	X_{RS}	1.37×10^{-2}	$(0.43, 3.57) \times 10^{-2}$
α/Ω	5.70×10^{-2}	$(3.50, 6.60) \times 10^{-2}$	X_{SI}	1.44×10^{-5}	$(2.94 \times 10^{-9}, 2.49 \times 10^{-4})$
Σ/Ω^2	5.58×10^{-7}	$(4.42, 0.10) \times 10^{-7}$	X_{RI}	6.24×10^{-6}	$(5.51 \times 10^{-9}, 2.45 \times 10^{-4})$
r	5.95×10^{-2}	$(5.20, 8.60) \times 10^{-2}$	X_{SR}	1.59×10^{-2}	$(0.28, 3.16) \times 10^{-2}$
			X_{IR}	7.61×10^{-6}	$(6.38 \times 10^{-10}, 6.48 \times 10^{-5})$

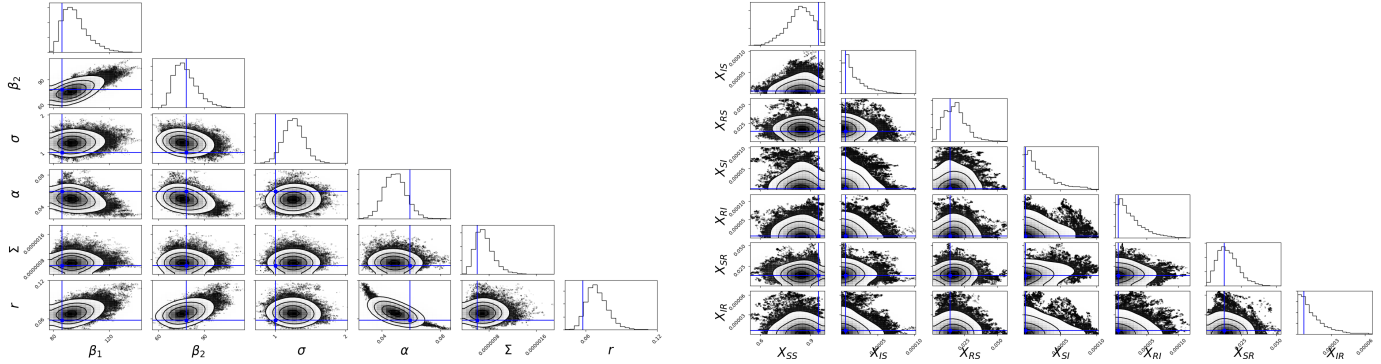


Figure 2: Pairwise marginal posterior plots for the model parameters (top panel) and initial conditions and auxiliary parameters (bottom panel) from the analysis in year 2003-04.

August 2004 - July 2005

Table 5: Posterior summaries for the analysis in year 2004-05

Parameter	MAP	95% HPD	Parameter	MAP	95% HPD
β_1	71.78	(64.87, 94.58)	X_{SS}	0.91	(0.64, 0.94)
β_2	69.84	(65.90, 95.31)	X_{IS}	3.49×10^{-7}	$(6.22 \times 10^{-11}, 2.31 \times 10^{-5})$
σ	0.37	(0.12, 0.872)	X_{RS}	0.01	(0.003, 0.031)
α/Ω	0.02	(0.008, 0.02)	X_{SI}	9.42×10^{-5}	$(6.68 \times 10^{-8}, 2.58 \times 10^{-4})$
Σ/Ω^2	4.76×10^{-7}	$(3.02, 7.28) \times 10^{-7}$	X_{RI}	6.80×10^{-5}	$(1.52 \times 10^{-8}, 2.46 \times 10^{-4})$
r	0.16	(0.13, 0.33)	X_{SR}	0.01×10^{-2}	(0.004, 0.04)
			X_{IR}	4.19×10^{-6}	$(1.40 \times 10^{-9}, 2.33 \times 10^{-5})$

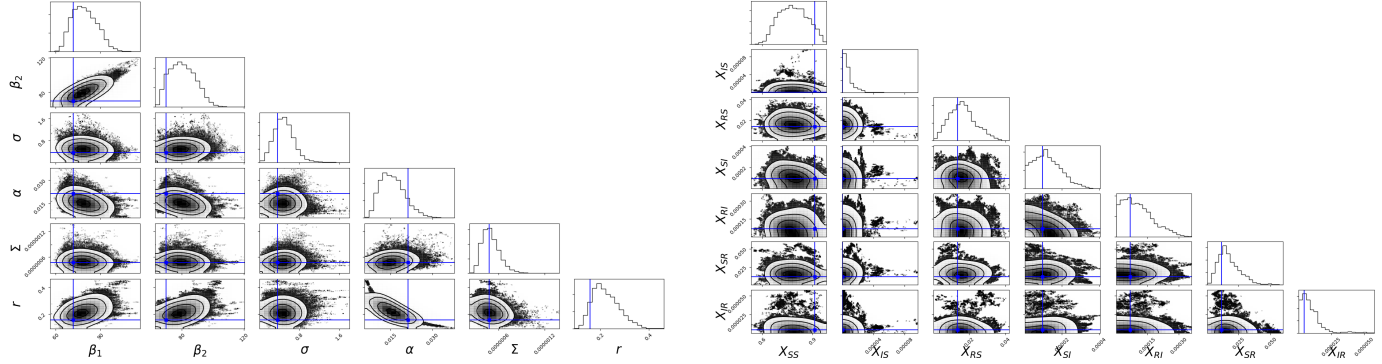


Figure 3: Pairwise marginal posterior plots for the model parameters (top panel) and initial conditions and auxiliary parameters (bottom panel) from the analysis in year 2004-05.

August 2005 - July 2006

Table 6: Posterior summaries for the analysis in year 2005-06

Parameter	MAP	95% HPD	Parameter	MAP	95% HPD
β_1	89.31	(70.45, 108.90)	X_{SS}	0.87	(0.63, 0.97)
β_2	89.24	(71.53, 110.09)	X_{IS}	4.17×10^{-6}	$(3.43 \times 10^{-10}, 4.48 \times 10^{-5})$
σ	0.19	(0.05, 0.43)	X_{RS}	0.01	(0.003, 0.03)
α/Ω	0.04	(0.013, 0.041)	X_{SI}	1.73×10^{-6}	$(1.36 \times 10^{-9}, 9.34 \times 10^{-5})$
Σ/Ω	8.32×10^{-7}	$(4.83 \times 10^{-7}, 1.18 \times 10^{-6})$	X_{RI}	1.67×10^{-5}	$(4.72 \times 10^{-9}, 1.21 \times 10^{-4})$
r	0.09	(0.08, 0.21)	X_{SR}	0.0098	(0.0027, 0.03)
			X_{IR}	5.59e-06	$(5.75 \times 10^{-10}, 8.14 \times 10^{-5})$

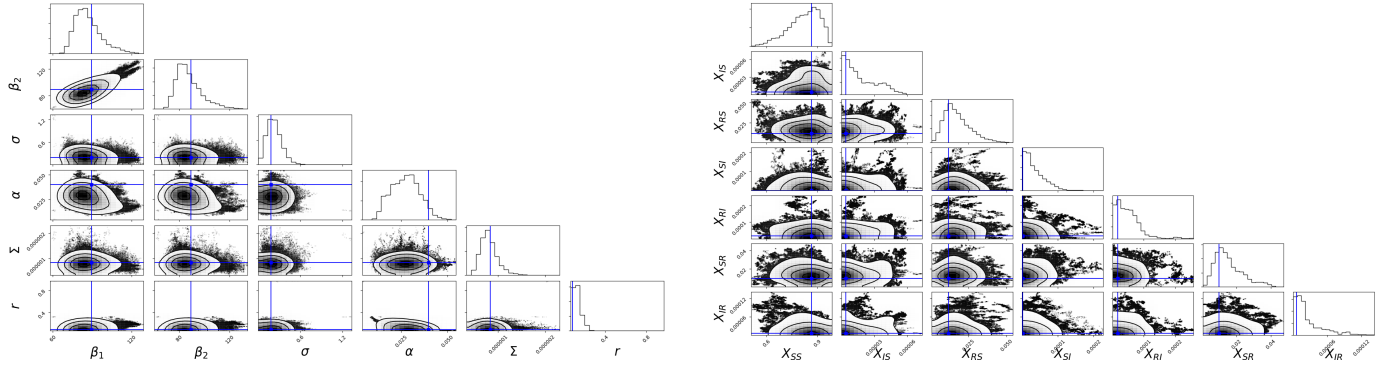


Figure 4: Pairwise marginal posterior plots for the model parameters (top panel) and initial conditions and auxiliary parameters (bottom panel) from the analysis in year 2005-06.

Table 7: Posterior summaries for the analysis in year 2006-07

Parameter	MAP	95% HPD	Parameter	MAP	95% HPD
β_1	74.26	(62.62, 99.95)	X_{SS}	0.85	(0.59, 0.95)
β_2	74.67	(64.50, 101.57)	X_{IS}	1.617e-07	(2.31×10^{-10} , 3.58×10^{-5})
σ	0.379	(0.09, 0.84)	X_{RS}	0.01	(0.005, 0.03)
α/Ω	0.016	(0.004, 0.02)	X_{SI}	6.23×10^{-5}	(2.35×10^{-10} , 2.36×10^{-4})
Σ/Ω^2	7.075×10^{-7}	(4.05, 9.9) $\times 10^{-7}$	X_{RI}	4.21×10^{-5}	(3.21×10^{-9} , 1.69×10^{-4})
r	2.12×10^{-1}	(0.14, 0.52)	X_{SR}	0.02	(0.003, 0.03)
			X_{IR}	8.43×10^{-6}	(8.94×10^{-7} , 3.23×10^{-5})

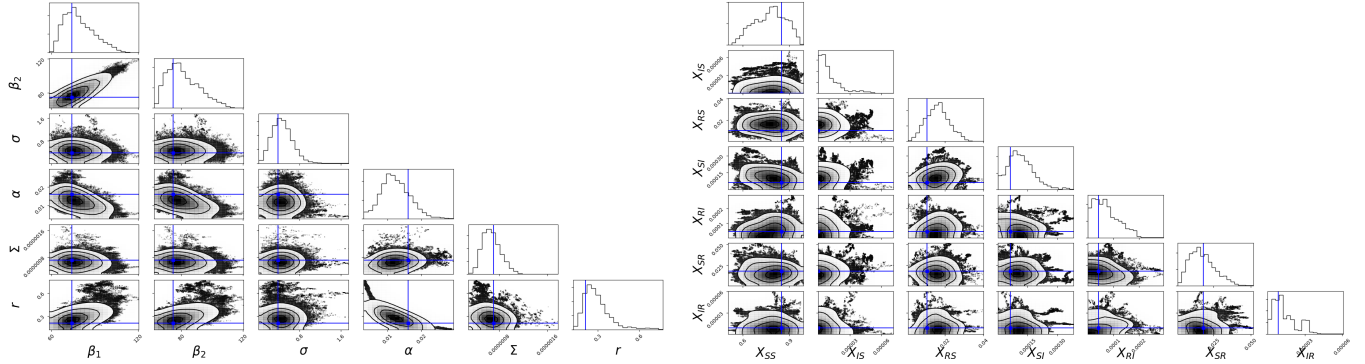


Figure 5: Pairwise marginal posterior plots for the model parameters (top panel) and initial conditions and auxiliary parameters (bottom panel) from the analysis in year 2006-07.

Table 8: Posterior summaries for the analysis in year 2007-08

Parameter	MAP	95% HPD	Parameter	MAP	95% HPD
β_1	79.12	(53.47, 97.79)	X_{SS}	0.746	(0.47, 0.91)
β_2	95.38	(77.11, 125.70)	X_{IS}	3.47×10^{-6}	$(3.69 \times 10^{-11}, 4.32 \times 10^{-5})$
σ	2.49	(1.46, 4.65)	X_{RS}	0.02	(0.007, 0.05)
α	0.09	(0.03, 0.10)	X_{SI}	2.79×10^{-5}	$(3.35 \times 10^{-9}, 1.78 \times 10^{-4})$
Σ	5.74×10^{-7}	$(3.68, 9.84) \times 10^{-7}$	X_{RI}	9.33×10^{-5}	$(3.13 \times 10^{-9}, 1.66 \times 10^{-4})$
r	0.04×10^{-2}	(0.032, 0.09)	X_{SR}	0.01	(0.003, 0.04)
			X_{IR}	5.97×10^{-7}	$(4.26 \times 10^{-12}, 4.07 \times 10^{-5})$

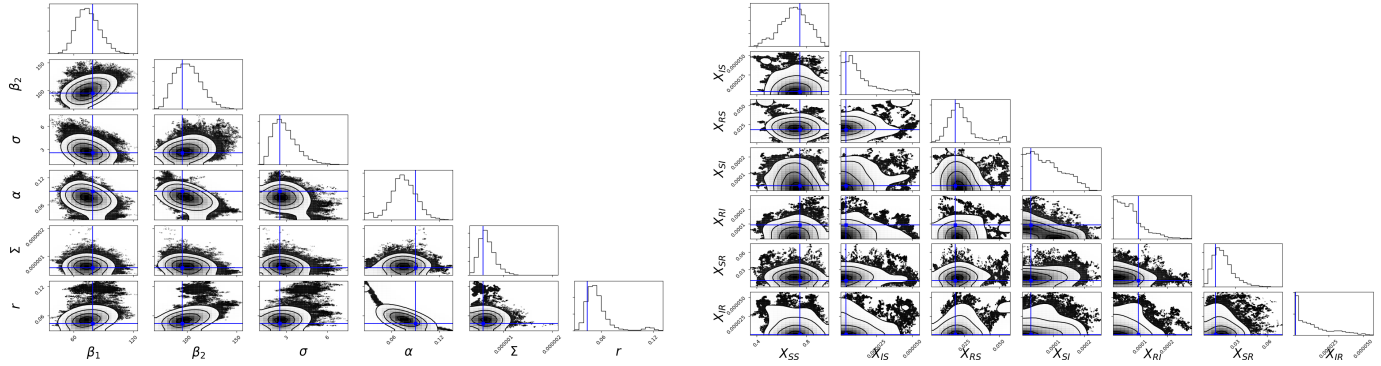


Figure 6: Pairwise marginal posterior plots for the model parameters (top panel) and initial conditions and auxiliary parameters (bottom panel) from the analysis in year 2007-08.

References

- Geyer, C. (1991). Markov chain Monte Carlo maximum likelihood. In *Computing Science and Statistics, Proceedings of the 23rd Symposium on the Interface*, 156. American Statistical Association.
- Gillespie, D. T. (2007). “Stochastic Simulation of Chemical Kinetics”. *Annu. Rev. Phys. Chem.*, 58:35–55.
- Golightly, A., Henderson, D. A., and Sherlock, C. (2015). “Delayed Acceptance Particle MCMC for Exact Inference in Stochastic Kinetic Models”. *Statistics and Computing*, 25(5):1039–1055.
- Kamo, M. and Sasaki, A. (2002). “The Effect of Cross-Immunity and Seasonal Forcing in a Multi-Strain Epidemic Model”. *Physica D: Nonlinear Phenomena*, 165(3):228–241.
- Van Kampen, N. G. (1992). *“Stochastic Processes in Physics and Chemistry”*, volume 1. Elsevier.